arXiv:astro-ph/0503681v1 31 Mar 2005

Filaments as Possible Signatures of Magnetic Field Structure in Planetary Nebulae[1]

P. J. Huggins & S. P. Manley

Physics Department, New York University, 4 Washington Place, New York NY 10003

patrick.huggins@nyu.edu, sm1006@nyu.edu

ABSTRACT

We draw attention to the extreme filamentary structures seen in high-resolution optical images of certain planetary nebulae. We determine the physical properties of the filaments in the nebulae IC 418, NGC 3132, and NGC 6537, and based on their large length-to-width ratios, longitudinal coherence, and morphology, we suggest that they may be signatures of the underlying magnetic field. The fields needed for the coherence of the filaments are probably consistent with those measured in the precursor circumstellar envelopes. The filaments suggest that magnetic fields in planetary nebulae may have a localized and thread-like geometry.

Subject headings: circumstellar matter — planetary nebulae: general — stars: AGB and post-AGB — stars: mass loss — stars: magnetic fields

1. Introduction

High-resolution imaging at optical wavelengths, especially with the Hubble Space Telescope (HST), has revealed a remarkable degree of complexity in the morphology of planetary nebulae (PNe). This includes both large and small scale structures such as multiple arcs, bubbles, bicones, point symmetric knots and bullets, tori, ansae, and globules (see, e.g., the recent volume edited by Meixner et al. 2004). The multiple arcs are formed in the precursor Asymptotic Giant Branch (AGB) phase (e.g., Mauron & Huggins 2000), but most of the other structures are thought to result from dynamical processes that take place in the circumstellar gas during the rapid transition from the AGB to the young PN phase.

[1]Based on observations made with the NASA/ESA Hubble Space Telescope, obtained from the data archive at the Space Telescope Institute. STScI is operated by the association of Universities for Research in Astronomy, Inc. under the NASA contract NAS 5-26555.

The possible role of magnetic fields in forming the complex structures seen in PNe is an area of ongoing debate. From a theoretical point of view, magnetic fields close to the central stars of PNe have been widely discussed in the context of models for launching bipolar jets which produce point symmetries, either from single stars or accretion disks in binaries (e.g., Frank & Blackman 2004; Garcia-Segura, Lopez, & Franco 2005). These models, however, are not currently very well constrained. The role of magnetic fields farther from the central stars has not been explored in detail. Early ideas were summarized by Pascoli (1985) who noted a possible connection between filaments and magnetic fields. More recent developments are described by Soker (2002; 2005) and references therein.

There are a growing number of observations of magnetic fields in PNe, but they do not yet form a complete picture. Magnetic fields in the central stars of PNe have very recently been detected for the first time, with kG fields (Jordan et al. 2005). In the extended nebulae, magnetic fields have been measured in a few young/proto-PNe using the polarization of maser spots in remnant circumstellar molecular gas (e.g., Miranda at al. 2001; Bains et al. 2004). More extensive measurements of maser spots have been made in the precursor circumstellar envelopes of AGB OH/IR stars (e.g., Vlemmings et al. 2002; Cotton et al. 2004). The masers extend from close to the stellar surface (in the case of the SiO masers in AGB stars) out to $\sim 10^{16}$ cm (for the OH masers), and in well observed cases the strength of the magnetic field is found to be significant, e.g., the plasma β parameter is $\lesssim 1$, where $\beta = 8\pi P_{\rm g}/B^2$, $P_{\rm g}$ is the gas pressure, and B is the magnetic field strength. However, the highly localized nature of the maser spots leaves uncertain the overall importance and geometry of the magnetic field. The orientation of the field can, in principle, be independently measured using the polarization of radiation from circumstellar dust grains. Sub-millimeter observations of the polarization in the young PN NGC 7027 and the proto-PN AFGL 2688 have been reported by Greaves (2002), although the angular resolution of the observations ($15''$) is too low to resolve the geometry.

In spite of the recent wealth of high-resolution imaging of PNe with the HST, there have so far been no compelling suggestions that these images provide direct evidence of magnetic field structures in the nebulae. Garcia-Segura et al. (2001) have proposed that the multiple arcs formed in the AGB phase and seen around PNe are caused by changes in the magnetic pressure, but this is still an open question. In contrast, in the case of the Sun, it is well known that high resolution images of the extended solar atmosphere provide some of the most direct and powerful diagnostics of the solar magnetic field. Although magnetic fields may be important close to the central stars in PNe, the commonly assumed situation is that the fields farther out are too weak to directly affect the structure of the nebulae on the size scales observed. For example, for a PN at 500 pc, an offset of $10''$ from the central star corresponds to a radial distance $\sim 5000\, R_*$, where R_*, the stellar radius, is taken to

be 1 A.U. for the AGB proto-PN transition. At this distance from the central star, the magnetic field is extremely small for a dipole radial variation ($B \sim r^{-3}$) and any plausible stellar surface field. However, a dipole variation may not be correct. The observations of the circumstellar envelopes of OH/IR stars indicate that the radial variation of the magnetic field in the maser spots may be less steep, $B \sim r^{-2}$ (Vlemmings et al. 2002; Vlemmings at al. 2005), and, under certain conditions, theoretical considerations suggest that the fall-off could be shallower, $B \sim r^{-1}$ (e.g., Pascoli et al. 1992; Chevalier & Luo 1994). Thus, the possible role of magnetic fields in the extended structure of PNe is an open question.

To explore this idea, we have examined high-resolution optical images obtained with the HST in order to search for possible signatures of the structural effects of magnetic fields in PNe. In this paper we present examples where we believe there is substantial evidence that the observed structure is the result of the underlying magnetic field. We estimate the magnetic field strengths, and discuss the implications.

2. Filaments as Signatures of the Magnetic Field

HST images of PNe, including the PNe discussed here, reveal a wealth of small scale structure, which is usually interpreted as the result of hydrodynamic processes involving the interactions of hot bubbles or jets with the surrounding circumstellar gas. The question we raise here is: if a magnetic field is present in the extended nebula, either advected, or already present in the circumstellar gas, what would be a morphological signature of its presence?

There is no straightforward answer to this question because there are no detailed, robust theoretical predictions. There are, however, general constraints from well observed examples and MHD simulations of related astrophysical environments. The dominant structure arising from the presence of a magnetic field in these cases is filamentary. Filaments are major structural features of the warm interstellar medium and cool molecular clouds. Most importantly there is the well observed case of the Sun where elongated magnetic structures – magnetic filaments or flux ropes – are the basic building blocks of the solar magnetic field. They are formed inside the Sun by the solar dynamo, they emerge through the solar surface in sunspots, they provide the complex helical structure of prominences, and form a component of the solar wind (see, e.g., Russell, Priest, & Lee 1990).

The magnetic field along a filament provides a connectivity in the gas that is not otherwise present. For this reason long filaments can remain coherent when accelerated non-uniformly; they can be twisted along their length; they can exhibit kinks or macroscopic writhe forming helices; and they can drape around and tangle with each other, until they

re-connect. These configurations are probably not easily produced by purely hydrodynamic processes. Two-dimensional simulations by Dwarkadas & Balick (1998) suggest that hydrodynamics can form types of filamentary structure in PNe, although those produced in the simulations typically appear short and oriented along the direction of wind interaction, unlike those discussed in this paper. We regard extreme filamentary structures, especially if they exhibit the characteristics described here, as likely signatures of the underlying magnetic field. In the following sections, we present examples of such filaments in three PNe.

3. Observations

The PNe that we consider, NGC 3132, IC 418, and NGC 6537, are all well known and have been studied at many wavelengths. Table 1 lists some basic parameters for orientation and later discussion. The distances (d), angular diameters ($\theta_{\rm D}$), and expansion velocities ($V_{\rm exp}$) are taken from Acker et al. (1992) or Gathier (1987), and the stellar temperatures (T_*) and electron densities ($n_{\rm e}$) are taken from Pottasch (2000), Pottasch, Bientema, & Feibelman (2000), Pottasch et al. (2004), Preite-Martinez et al. (1991), and Gathier (1987). The values of $n_{\rm e}$ are characteristic of values found from emission line ratios and from the intensities of the Balmer lines or the radio continuum. The expansion timescales are given by $t_{\rm exp} = \theta_{\rm D} d/(2V_{\rm exp})$.

The three PNe are young or middle-aged (2,000–4,000 yr), but the wide range in temperature of the central stars indicates different evolutionary stages and/or different core masses. The morphologies are also different (see Section 4). All are relatively nearby, so that the features we describe are likely to be characteristic of a wide range of more distant objects in the PN population.

The observations that we discuss were obtained with the Wide Field and Planetary Camera (WFPC2) on board the HST. The data were retrieved from the HST archives, and have been processed through standard pipelines. Details of the exposures are given in Table 2. The pixel size is $0\farcs05$ for the images of IC 418, and $0\farcs10$ for those of NGC 3132 and NGC 6537. Images of all three PNe have been reported in HST press releases, and NGC 3132 and IC 418 appear in the Hubble Heritage gallery. However, to our knowledge, none of these data have been described in detail in the astronomical literature. Our objective is not to present the complete HST data sets, but to focus on specific features of the nebulae.

4. Properties of the Filaments

4.1. NGC 3132

NGC 3132 is known as the Southern Ring Nebula because it has a morphology that is somewhat similar to its northern counterpart NGC 6720. An overview of its structure is shown in Fig. 1. The feature of interest is the bar or ridge which forms a chord across the main ring, and appears to be a remnant of a thin torus. It lies nearly vertical, to the left of the bright star near the center in Fig. 1.

High resolution HST images (see Table 2) of the upper part of this feature in [O III] λ5007 and [N II] λ6583 are shown Fig. 2. The left hand panels are direct images with logarithmic intensity scales (shown next to each) to cover the full dynamic range of the data. The right hand panels are unsharp mask images that reduce background variations and emphasize the small scale structure. The unsharp mask versions were formed from the ratio $I_o/(I_{\rm s} + 0.05I_{\rm o})$ where $I_{\rm o}$ is the original image and $I_{\rm s}$ is a smoothed image, made using a Gaussian of FWHM 14 pixels.

In the [O III] λ5007 image, the bar is seen mainly in absorption by dust grains. The bar lies in front of most of the O III ionization zone along the line of sight, and the [O III] λ5007 emission serves as background illumination for absorption by the dust in the bar. In contrast, the N II ionization zone extends farther from the central star and includes the bar region, so that the image in [N II] shows emission from the bar, as well as dust absorption.

Inspection of the images shows that the bar is not monolithic. It consists of several related, thin filaments. One prominent filament, seen in absorption in the upper left of the [O III] image, is relatively straight; it turns through an angle of $\sim 50^\circ$ at the location of the knot which lies just above the center of the image, and continues straight along the length of the bar. Parts of the edges of this filament are seen bright in [N II]. A second prominent and sinuous filament seen in the [O III] image in the upper right, connects with the knot, and appears to spiral around the taut filament along the length of the main bar. A third filament, bright in [N II] and distinctly kinked, connects with the knot from the top, although the geometry of its continuation is unclear. Other, less prominent filaments, including a distinct loop above the knot, connect to these main features.

The well-defined absorption in the [O III] λ5007 image makes it very useful for determining the properties of the filaments. Horizontal intensity cuts across the image are shown in Fig. 3 to illustrate the widths and depths of the absorption. The widths (FWHM) of the more prominent strands are $0\farcs2 - 0\farcs6$ and somewhat larger at the main knots or kinks. At the distance of NGC 3132 (Table 1), a representative width of $0\farcs4$ corresponds to 3.6×10^{15} cm.

This subtends an angle of only $\sim 1^\circ$ at the central star. The longest filament can be traced more than a quarter of the way around the nebula, and has a length/width ratio of $\gtrsim 60$.

We estimate the density in the filaments from the depths of the dust absorption. The peak absorption ranges up to ∼50–70% for the most prominent kinks and knots, and we adopt a value of 20% as representative of a typical, single filament. At the wavelength of the [O III] λ5007 line, this corresponds to a color excess $E(\mathrm{B-V})$ of 0.08, and a hydrogen column density $N(\mathrm{H\ I} + \mathrm{H_2})$ of 5×10^{20} cm^{-2}, using the relation $N(\mathrm{H\ I} + \mathrm{H_2}) = 5.8 \times 10^{21} E(\mathrm{B-V})$ from Bohlin, Savage, & Drake (1978). For a line of sight depth equal to the typical width of a filament given above, the density is 1.3×10^5 cm^{-3}, much higher than the average electron density given in Table 1. The gas in the filaments can be expected to range from ionized at the surface to molecular in the core. H_2 emission can be seen along the bar in the data of Allen et al. (1997), although it is not well resolved. The situation is probably like that in the globules of the Helix Nebula (Huggins et al. 2002). There is likely to be a range in temperature from the surface to the core, and if we adopt an intermediate state of neutral atomic gas at a temperature of 100 K, the pressure is 1.8×10^{-9} dyne cm^{-2}.

The properties of the filaments in NGC 3132 described above place strong constraints on possible formation scenarios. Based on purely hydrodynamic considerations the matter ejected in the precursor AGB wind is expected to be smoothed out on the smallest angular sizes scales in the acceleration region (Huggins & Mauron 2002). The filaments lie at larger distances from the central star and they are oriented tangentially. They cannot be produced at their current location as wind swept tails, and are unlikely to be produced by hydrodynamic instabilities such as the Rayleigh-Taylor or nonlinear thin-shell instabilities as modeled by Dwarkadas & Balick (1998), where the structure is typically short and oriented along the direction of the wind interaction. Tangential optical filaments are pervasive in evolved supernova remnants, and are generally interpreted as thin sheets of emission, seen edge-on (Raymond et al. 1988). In PNe, similar effects are commonly seen as limb-brightened bubble surfaces, but other linear features (see, e.g., O'Dell et al. 2002) may be similar to those discussed here. In NGC 3132 the images show that the filaments are long, thin physical structures, and together they form a vestigial ring or torus. They might arise from some shearing instability, but the extreme thread-like character of the filaments together with their local kinked and looped geometry lead us to propose that their structure is dominated by a magnetic field. The most likely scenario is that they were formed in the early development of the PN close to the star, possibly in a magnetized torus in the proto-PN phase, and their coherence has been maintained by the influence of the longitudinal field.

4.2. IC 418

IC 418 is a well-studied, compact PN with a high surface brightness in the Balmer lines and the radio continuum. An overview of the structure in Hα is shown in Fig. 4. In addition to the classic elliptical morphology with enhanced intensity along the minor axis, it exhibits complex, small scale structure in the form of filaments and blisters. This is seen more clearly in the unsharp mask image (made in the same way as described in the previous section) shown in the top left panel of Fig. 5.

The filaments in IC 418 are brighter than the background nebula emission in Hα, which indicates that they consist of higher density gas. Individual filaments can be traced over distances comparable to the diameter of the nebula, and in certain areas they form a semi-regular grid pattern. The blistered regions probably occur where the ionized gas in the interior of the nebula has pushed through the pattern. The globally co-ordinated structure indicates that the grid pattern was formed by ejection from the center over time, with a gradual change in the orientation of the ejection. A more detailed model will be reported in a separate paper.

The thread-like nature of the filaments and their local geometry can be seen in the close-up unsharp mask images in Fig. 5. The two panels on the right show the same field in Hα and [N II] λ6583, centered below and to the left of the central star (as seen in the full image) where the pattern is clearest. The bottom-left panel shows the enlarged center of this field in Hα. The images have been smoothed with a Gaussian of width (FWHM) 2 pixels to improve the visibility without significant loss of detail. The pattern in the images is mostly formed by enhanced emission from the filaments, although there are also parts of filaments where absorption or geometric effects due to the oblique illumination by the central star give a diminution of the light. The filaments can be expected to be at different distances along the line of sight, but many span a large angular extent and reach the edges of the nebula, which indicates that they are typically near the surface. The bright feature seen in the top right corner of the intermediate scale Hα image is part of an interior ring around the central star, and is not seen in [N II] because the N II ionization zone begins farther from the star. Most of the other features can, however, be traced point by point with slight differences in Hα and [N II], which argues strongly that they trace real structural elements. The HST image in [O III] λ5007 (not displayed here) shows a diffuse nebula with the inner ring and a few filaments in emission, together with evidence of dust absorption, but not sufficiently clearly for systematic measurements as in NGC 3132.

The typical widths of bright individual strands (measured on the original Hα image) are ~ 3 pixels ($0\farcs14$), which corresponds to 2×10^{15} cm at the distance of IC 418. The strands subtend an angle of only $\sim 1^\circ$ at the central star, and those that can be traced over more

than half the diameter of the nebula have length/width ratios $\gtrsim 40$.

The density in the filaments can be estimated by measuring the intensity enhancement (ΔI) across a strand relative to the average background emission of the nebula (I). Since the intensities depend upon the emission measure along the line of sight, the electron density in the filament ($n_{\rm f}$) is related to the average density in the nebula $n_{\rm n}$ (assuming uniform conditions) by the equation $n_{\rm f} = n_{\rm n}(\Delta I d_{\rm n}/I w_{\rm f})^{1/2}$, where $w_{\rm f}$ is the filament width (ignoring orientation effects) and $d_{\rm n}$ is the depth of the nebula along the line of sight. Using the thickness of a filament given above, the dimensions of the nebula from Table 1, and a filament/nebula intensity contrast ($\Delta I/I$) of 10%, which is representative of the brighter filaments, we find $n_{\rm f} \sim 3n_{\rm n}$. Using the value of $n_{\rm n}$ given in Table 1 and a temperature of 10^4 K, the gas pressure in the filaments is 1.0×10^{-7} dyne cm^{-2}. IC 418 is not detected in molecular line emission (Huggins et al. 1996), but it is seen in the H I 21 cm line (Gussie et al. 1995). The nebula is not resolved at 21 cm, so it is uncertain if the filaments have neutral atomic cores; Gussie et al. (1995) interpret the H I emission as arising from a neutral halo.

The global pattern of the filaments in IC 418 rules out shell instabilities as a plausible formation scenario. The extreme thread-like character of the filaments and their curved, spaghetti-like geometry, which includes partial loops or helical writhe, makes a strong case that they are magnetically dominated structures. The filaments might be formed primarily from material in the nebula shell, where it has been locally compressed to higher density by the action of jets from the central star. However, the narrow angle subtended at the center ($\sim 1^\circ$), which would imply unusually high collimation for the jets, and the local geometry probably rule this out. The most likely formation scenario is one in which the filaments were ejected over time as continuous or intermittent strands, or multiple loops, from the central star.

4.3. NGC 6537

NGC 6537 is a bipolar/butterfly PN with an extremely hot central star (Table 1). The nebula extends $\sim 120''$ from the center and is formed by high velocity (300 km s^{-1}) outflows (Corradi & Schwartz 1993) which show complex structure. The region of interest here is the $5''$ core of the nebula, which is shown in Hα and [N II] λ6583 in Fig. 6. The axis of the extended nebula is roughly orthogonal to the axis of the core, but its structure indicates that the outflows are directed at considerable angles from the main axis, and emerge obliquely from the core region, as seen, e.g., in ablated gas extending toward the top right in Fig. 6.

The core of NGC 6537 does not show such extreme filaments as the cases discussed

above, but is of interest as an example of a relatively complete equatorial torus showing filamentary sub-structure. The torus is not axi-symmetric, but three main components can be discerned: a kinked, main ring (roughly horizontal in the figure), and two distorted, tilted, semi-circular filaments, linked or embedded in the walls of the torus above and below the ring. The structure seen in Hα and [N II] is nearly the same; the main difference being the absence of [N II] emission from the center, where the nitrogen is in higher ionization states because of the high stellar temperature. Images in [O III] λ5007 and [O I] λ6300 (not shown) are roughly similar.

The thickness of the filaments ranges from $\lesssim 0\farcs2$ (unresolved) to $\sim 0\farcs5$ ($\lesssim 7 \times 10^{15}$ cm to 1.8×10^{16} cm), and they subtend angles at the center of $\lesssim 5°$ to $\sim 12°$, so they are generally larger structural elements of the nebula than in the previous cases discussed. The length/width ratio, assuming semi-circles with the radius of the horizontal ring, ranges from 16 to $\gtrsim 40$. The filaments dominate the line emission from the core of NGC 6537 so the density in Table 1 is representative of the density in the bright ionized regions seen in Fig. 6. The corresponding gas pressure is 2.8×10^{-8} dyne cm^{-2}. The central regions of NGC 6537 show CO emission (Huggins et al. 2005) which probably implies that the filaments have molecular cores below the photo-ionized surfaces.

The expansion velocity of the torus is 18 km s^{-1} (Table 1) and its expansion time scale (1,600 yr) is comparable to that of the much more extended nebula formed by the high velocity outflows. The torus represents the last major mass ejection by the central star. The ejection was sudden, there is no radially extended equatorial disk, and the mass is substantial, ~ 0.02 M$_\odot$ in ionized gas alone (estimated from the parameters in Table 1). The low velocity of the torus and the continuity of the filaments over large angles in longitude suggests that they were formed during the ejection process. Their distortion is probably a result of interaction with the high velocity outflows since the upper filament is evidently being ablated. The arguments that the filaments are held together with a magnetic field follow those for NGC 3132. The conclusion is less compelling than in the previous cases where the filamentary structures have such extreme geometries, but is still the most reasonable explanation of their structure.

5. Discussion

5.1. Field Strengths

Our interpretation of the geometry of the filaments described above is that they provide morphological evidence for the influence of magnetic fields in the extended structure of PNe.

If this is correct, the properties of the filaments can be used as a guide to the likely field strengths.

The most important consideration for the integrity of a filament in the expanding PN environment is its connectivity. Using a very simple picture ignoring the effects of vorticity, the breaking time of a non-magnetic, tangential filament is given by $t_{\rm b} = w_{\rm f}/\Delta V$ where ΔV is the velocity of any radial shear. For $\Delta V = V_{exp}$ (~ 18 km s^{-1}), $t_{\rm b}$ is 50 yr, much shorter than the expansion time of the nebulae ($\sim 3,000$ yr). Even if ΔV is as low as 1 km s^{-1}, which may be typical of the turbulent velocity in the cool precursor envelope (e.g., Huggins & Healy 1986), $t_{\rm b}$ is still less than the expansion time scale. Thus, unless the filament is connected along its length, it is likely to break.

A second consideration for the integrity of a filament is its lateral dispersion. However, this is a less crucial issue. From the observations we cannot determine the extent to which a filament is in close pressure equilibrium with its surroundings, so for illustration we consider free expansion, for which the dispersion time scale is $t_{\rm d} = w_{\rm f}/2c_{\rm s}$ where c_s is the sound speed. Although $t_{\rm d}$ is short (~ 50 yr) compared with the expansion time scales of the nebulae if the gas is ionized ($c_s \sim 10$ km s^{-1}), it is probable that the filaments of NGC 3132 and NGC 6537, and possibly IC 418, have neutral, low temperature cores with low sound speeds. In this case the ionized gas seen in the images forms a thin skin or a photo-evaporation flow from the surface of the filament. Even if this gas is not confined and disperses on short time scales, a filament can maintain its thin lateral dimension as long as the ionization front is weak, and the cool, neutral core is maintained.

Two standard parameters describe the importance of a magnetic field in the PNe and are relevant to the integrity of a filament: β, the ratio of the thermal gas pressure to the magnetic pressure, defined in section 1, and σ, the ratio of the magnetic energy density to the kinetic energy density, i.e., $\sigma = B^2/(4\pi\rho V_{\rm exp}^2)$ where ρ is the gas density. Using the gas densities and gas pressures in the filaments determined in the previous sections and the values of $V_{\rm exp}$ from Table 1, we calculate the strength of the fields ($B_{\rm P}$) for which $\beta = 1$, and the strength of the fields ($B_{\rm E}$) for which $\sigma = 1$. The results are given in Table 3, together with representative distances of the filaments from the central stars. It can be seen from the table that these values of the fields are not very different from one another (~ 1 mG).

A field with $\sigma \sim 1$ would dominate the overall dynamics of a filament and would render it extremely stiff against perturbations. A field with $\beta \sim 1$ would also play a role in the local behavior of a filament, and with the appropriate helical geometry would help or dominate the confinement (e.g., Fiege & Pudritz 2000). However, fields estimated on the basis of equipartition are probably upper limits because of the high magnetic tension (see also Soker 2005). The magnetic tension force is given by $T_{\rm M} = B^2/4\pi R_{\rm c}$ per unit volume, where $R_{\rm c}$ is

the radius of curvature of the field. For a filament at radius r expanding with velocity $V_{\rm exp}$, the tension force can be expressed as $T_{\rm M} = \sigma\rho V_{\rm exp}^2/r$, and for $\sigma = 1$, it can be seen to be sufficiently large to arrest the motion of the filament on a time scale equal to the expansion time scale ($r/V_{\rm exp}$), unless there is also a strong, outwardly directed gradient in the field. The observed filaments do not currently appear to have a separate dynamical evolution from other parts of the nebulae.

A more realistic scenario is one in which the magnetic field plays a dynamical role closer to the central star where the fields might be relatively stronger. For example, $\sigma \lesssim 1$ at some representative radius $r_{\rm a}$ where the filaments are formed and/or the gas is accelerated to its terminal velocity. We do not know how the field has varied with distance from the star, but if we assume that the gas density at $r_{\rm a}$ is related to the observed density by $\rho_{\rm a} = \rho(r/r_{\rm a})^2$ and the velocity is $\sim V_{\rm exp}$, we can estimate the equi-partition field at r_a. The results for a representative radius of $r_{\rm a} = 10^{15}$ cm are given in Table 4, labeled $B_{\rm E}(10^{15})$.

An alternative scenario is one in which the magnetic field plays a subordinate role in the overall dynamics, but the magnetic tension plays a cohesive role on small length scales (see also Soker 2002). From the expression given above ($T_{\rm M} = \sigma\rho V_{\rm exp}^2/r$), it can be seen that even with $\sigma \ll 1$ the tension that results from small scale ($\ll r$) perturbations can be large. For example, if a filament is subject to disruptive forces that would produce variations in the terminal velocity of $\sim V_{\rm exp}/10$ on length scales of $\sim r/10$ in an expansion time, the disrupting forces can be effectively balanced by the tension if the field is $\gtrsim B_{\rm E}(r)/10$. Thus fields significantly smaller than equi-partition fields can still provide strong, local connectivity along the length of a filament.

5.2. Comparison with Observed Fields

The magnetic fields estimated on the basis of equi-partition in the previous section are plotted against radius in Figure 7. For comparison we show the fields measured in the maser spots of circumstellar envelopes, as presented by Vlemmings et al. (2002). The boxes show the fields from SiO and OH masers in Mira variables (dashed lines) and supergiants (solid lines), and the dashed and solid lines indicate corresponding $B \sim r^{-2}$ fits to the radial variation of the field. The typical precursor of a PN at the tip of the AGB probably lies somewhere near the supergiant data. The OH masers of the two proto-PNe discussed by Bains et al. (2004) have fields of ~ 3 mG at radii of 6×10^{15} cm and 3×10^{16} cm, and lie inside the supergiant OH maser box. Recent observations of H_2O masers by Vlemmings et al. (2005) suggest a dipole (r^{-3}) field rather than an r^{-2} field in the supergiant VX Sgr, but this does not change the overall picture presented here.

Could the PN filaments have developed from the fields seen in the precursor envelopes? It can be seen from Fig. 7 that the current equi-partition fields in the filaments are comparable to those in the OH masers in the envelopes, and they lie farther from the central star by about an order of magnitude. They therefore lie above the solid line in the figure by 1–2 orders of magnitude. Although we regard the equi-partition fields as likely overestimates, fields of this magnitude can probably be produced at their current distances from the star by the compression of the neutral gas in the AGB envelopes when overtaken by the ionization front of the nebula, with a corresponding increase in the field (e.g., Soker 2002). More importantly, when we consider the field estimates at the acceleration region closer to the star, the equi-partition fields of the PN filaments are comparable to the observed maser fields, and subordinate but cohesive fields (as discussed above) are even lower. We therefore conclude that the fields needed to play a role in the development of PN filaments could have originated in the precursor circumstellar gas.

For completeness, we note that a PN central star with an average surface field of 1.5 kG and a radius 0.3 $R_{\odot}$, comparable to the cases recently reported by Jordan et al. (2005), would likely produce weak fields in the extended nebula. For example, a variation of r^{-2} from the surface would fall about three orders of magnitude below the dashed line in Fig. 7. This could be increased by a less steep (r^{-1}) radial dependence and/or shock compression, but the relation of the observed stellar field to that of the AGB stars is not yet clear. The geometry suggested by the filaments may be important in developing this picture.

5.3. Geometry

Our suggestion that the filaments may be identified with the underlying magnetic field structure in the nebulae is of interest because there are currently no other guides to the detailed geometry of the fields in PNe. The PNe considered here have different overall morphologies, but they share a common characteristic of localized structures with long-range longitudinal coherence, i.e., they are stringy. This is rather different from the relatively smooth fields that are typically used in theoretical models of magnetic fields in PNe and may indicate that high resolution simulations are needed to produce realistic models. Of course the PNe were selected on the basis of their filaments, so they may be isolated, peculiar cases. However, they are all relatively nearby objects, and their other properties are quite typical of PNe, so they may be representative of a wide distribution of the PN population.

In all three PNe the filaments are roughly perpendicular to the radius vector. This is consistent with the dominance of tangential magnetic fields at large distances from the central stars as expected on general theoretical considerations (e.g., Pascoli et al. 1992; Chevalier &

Luo 1994). The filaments in IC 418 and NGC 3132 are very thin with large length-to-width ratios, and this may be also be the case in NGC 6537 but it is more distant so that any small scale structure is not resolved in the images. The filaments in NGC 6537 and NGC 3132 are parts of rings or tori, which are made up of more than one filament. Rings and tori are very common in PNe, and they may have similar substructure when observed at high spatial resolution. The case of IC 418 is different in that it involves time dependent changes in the direction of ejection, but the underlying mechanisms may be similar.

There are no detailed theoretical predictions of the local geometry of the magnetic field in PNe. However, based on analogy with the case of the solar field and magnetic clouds (e.g., Russell, Priest, & Lee 1990) and models for filamentary clouds in the interstellar medium (e.g., Fiege & Pudritz 2000), we expect that the filaments are in the form of magnetic flux ropes, with longitudinal fields in the core, surrounded by azimuthal components farther from the axis. It may be possible to investigate this directly with additional observations.

The geometry of the filaments and the likely field strengths discussed in previous sections lead naturally to the possibility that the OH maser spots in circumstellar envelopes may be regions of enhanced gas density and magnetic field associated with proto-filaments. The recent suggestion from a different perspective by Soker & Kastner (2003) that the maser spots in AGB envelopes represent local enhancements of the magnetic field, is consistent with this idea. However, there is a sharp transition from roughly spherical mass loss on the AGB to toroidal structures in proto-PNe: if magnetic fields play an important role in this transition, the filaments that we describe here, especially the toroidal ones, could also be the products of this enhanced magnetic activity.

6. Conclusions

The HST observations reported in this paper provide a means of exploring the potential connection between filaments and magnetic fields in PNe, a possibility mentioned two decades ago by Pascoli (1985). The high resolution images provide striking examples of extreme filamentary structures. The thread-like character and geometry of the filaments lead us to propose that they may be signatures of the underlying magnetic field. We have derived the physical properties of the gas in the filaments, and find that fields which would be strong enough to provide coherence, are probably consistent with those measured in the precursor circumstellar envelopes. The filaments suggest that the magnetic fields in PNe may be localized and thread-like.

We thank Dr. Adam Frank and an anonymous referee for helpful comments. This work

has been supported in part by NSF grant AST 03-07277 (to P.J.H.).

REFERENCES

Acker, A., Ochsenbein, F., Stenholm, B., Tylenda, R., Marcout, J., & Schohn, C. 1992, The Strasbourg-ESO Catalog of Galactic Planetary Nebulae (Garching: ESO)

Allen, L. E., Ashley, M. C. B., Ryder, S. D., Storey, J. W. V., Sun, Y.-S., & Burton, M. G. 1997, Planetary nebulae, IAU Symposium 180, Ed. H. J. Habing & H. J. G. L. M. Lamers, (Dordrecht: Kluwer), 205

Bains, I., Richards, A. M. S., Gledhill, T. M., & Yates, J. A. 2004, MNRAS, 354, 529

Bohlin, R. C., Savage, B. D., & Drake, J. F. 1978, ApJ, 224, 132

Chevalier, R. A., & Luo, D. 1994, ApJ, 421, 225

Corradi, R. L. M., & Schwarz, H. E. 1993, A&A, 269, 462

Cotton, W. D., et al. 2004, A&A, 414, 275

Dwarkadas, V., & Balick, B. 1998, ApJ, 497, 267

Fiege, J. D., & Pudritz, R. E. 2000, MNRAS, 311, 85

Frank, A., & Blackman, E. G. 2004, ApJ, 614, 737

Garcia-Segura, G., Lopez, J. A., & Franco, J. 2001, ApJ, 560, 928

Garcia-Segura, G., Lopez, J. A., & Franco, J. 2005, ApJ, 618, 919

Gathier, R. 1987, A&AS, 71, 245

Greaves, J. S. 2002, A&A, 392, L1

Gussie, G. T., Taylor, A. R., Dewdney, P. E., & Roger, R. S. 1995, MNRAS, 273, 790

Huggins, P. J., & Healy, A. P. 1986, ApJ, 304, 418

Huggins P. J., Bachiller R., Cox P., & Forveille T. 1996, A&A, 315, 284

Huggins, P. J., Forveille, T., Bachiller, R., Cox, P., Ageorges, N., & Walsh, J. R. 2002, ApJ, 573, L55

Huggins, P. J., & Mauron, N. 2002, A&A, 393, 273

Huggins, P. J., Bachiller, R., Planesas, P., Forveille, T. & Cox, P. 2005, ApJS, submitted

Jordan, S., Werner, K., & O'Toole, S. J. 2005, A&A, 432, 273

Mauron, N., & Huggins, P. J. 2000, A&A, 359, 707

Meixner, M., Kastner, J, H., Balick, B., & Soker, N. 2004, ASP Conf. Ser. 313, Asymmetrical Planetary Nebulae III: Winds, Structure and the Thunderbird, ed. M. Meixner, J. H. Kastner, B. Balick, & N. Soker (San Francisco: ASP)

Miranda, L. F., Gomez, Y., Anglada, G., & Torrelles, J. M. 2001, Nature, 414, 284

O'Dell, C. R., Balick, B., Hajian, A. R., Henney, W. J., & Burkert, A. 2002, AJ, 123, 3329

Pascoli, G. 1985, A&A, 147, 257

Pascoli, G., Leclercq, J., & Poulain, B. 1992, PASP, 104, 182

Pottasch, S. R. 2000, A&A, 362, L17

Pottasch, S. R., Beintema, D. A., & Feibelman, W. A. 2000, A&A, 363, 767

Pottasch, S. R., Bernard-Salas, J., Beintema, D. A., & Feibelman, W. A. 2004, A&A, 423, 593

Preite-Martinez, A., Acker, A., Koeppen, J., & Stenholm, B. 1991, A&AS, 88, 121

Raymond, J. C., Hester, J. J., Cox, D., Blair,,W. P., Fesen, R. A., & Gull, T. R. 1988, ApJ, 324, 869

Russell, C. T., Priest, E. R., & Lee, L. C. 1990, Physics of Magnetic Flux Ropes (Washington: AGU)

Soker, N. 2002, MNRAS, 336, 826

Soker, N. 2005, preprint(astro-ph/0501647)

Soker, N., & Kastner, J. H. 2003, ApJ, 592, 498

Vlemmings, W. H. T., Diamond, P. J., & van Langevelde, H. J. 2002, A&A, 394, 589

Vlemmings, W. H. T., van Langevelde, H. J., & Diamond, P. J., 2005, preprint(astro-ph/0501628)

This preprint was prepared with the AAS LaTeX macros v5.2.

Table 1. PN Properties

PN	Name	d (kpc)	$\theta_{\rm D}$ ($''$)	$n_{\rm e}$ (cm^{-3})	T_* (K)	$V_{\rm exp}$ (km s^{-1})	$t_{\rm exp}$ (yr)
010.1+00.7	NGC 6537	2.4	10	10,000	$\gtrsim$500,000	18	3,200
215.2−24.2	IC 418	1.0	12	12,000	33,000	12	2,400
272.1+12.3	NGC 3132	0.6	56	700	99,000	21	3,800

Table 2. Image Information

PN	Dataset	Filter	Exp. Time (s)
NGC 3132	U5HC0101B	F502N	800
	U5HC0103B	F658N	700
IC 418	U35T0905B	F656N	880
	U66B1006B	F658N	700
NGC 6537	U42I0402B	F656N	1240
	U42I0407B	F658N	1200

Table 3. Equi-partition Magnetic Fields

PN	r (10^{16} cm)	$B_{\rm P}(r)$ (mG)	$B_{\rm E}(r)$ (mG)	$B_{\rm E}(10^{15})$ (mG)
NGC 6537	9	0.84	0.82	74
IC 418	9	1.60	1.00	94
NGC 3132	18	0.21	3.47	624

Fig. 1.— Overview image of NGC 3132, adapted from the Hubble Heritage image. The field is $87'' \times 61''$. North is 109° counter-clockwise from vertical.

Fig. 2.— Filaments in NGC 3132. *Left*: Images in [O III] λ5007 (top) and [N II] λ6583 (bottom) with logarithmic intensity scales. *Right*: Unsharp mask versions of these images (see text for details). The fields are $12'' \times 19''$.

Fig. 3.— Intensity cuts in [O III] λ5007 through the filaments of NGC 3132. The strips are horizontal cuts through the image in Fig. 2. They are labeled with the vertical distance in arc seconds from the knot feature, and are offset along the intensity axis for clarity.

Fig. 4.— Overview image of IC 418 in Hα. The field is $18'' \times 18''$. North is 117° clockwise from vertical.

Fig. 5.— Filaments in IC 418. *Top left*: Hα, field $18'' \times 18''$. *Top right*: Hα, field $4\farcs7 \times 4\farcs7$. *Bottom right*: [N II] λ6583, field $4\farcs7 \times 4\farcs7$. *Bottom left*: Hα, field $2\farcs9 \times 2\farcs9$. All panels are unsharp mask images, smoothed with a FWHM of 2 pixels.

Fig. 6.— Images of the torus of NGC 6537 in Hα (top) and [N II] λ6583 (bottom). The greyscale is inverted. The field is $9'' \times 8''$, north is 45° counter-clockwise from vertical.

Fig. 7.— Magnetic field strength versus radius for evolved stars and PNe. The equi-partition fields of the PNe from Table 3 are denoted by crosses ($B_{\rm P}$), filled triangles ($B_{\rm E}$) and open triangles ($B_{\rm E}$ at 10^{15} cm). The boxes denote the ranges for SiO and OH masers for Miras (dashed lined) and supergiants (solid line), and the solid and dashed lines are r^{-2} fits through these from Vlemmings et al. (2002).

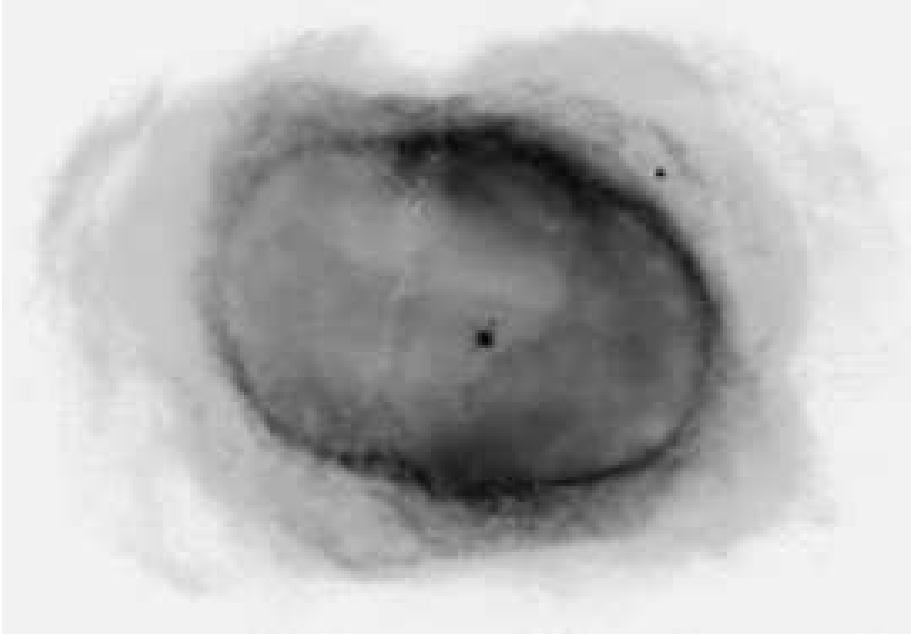

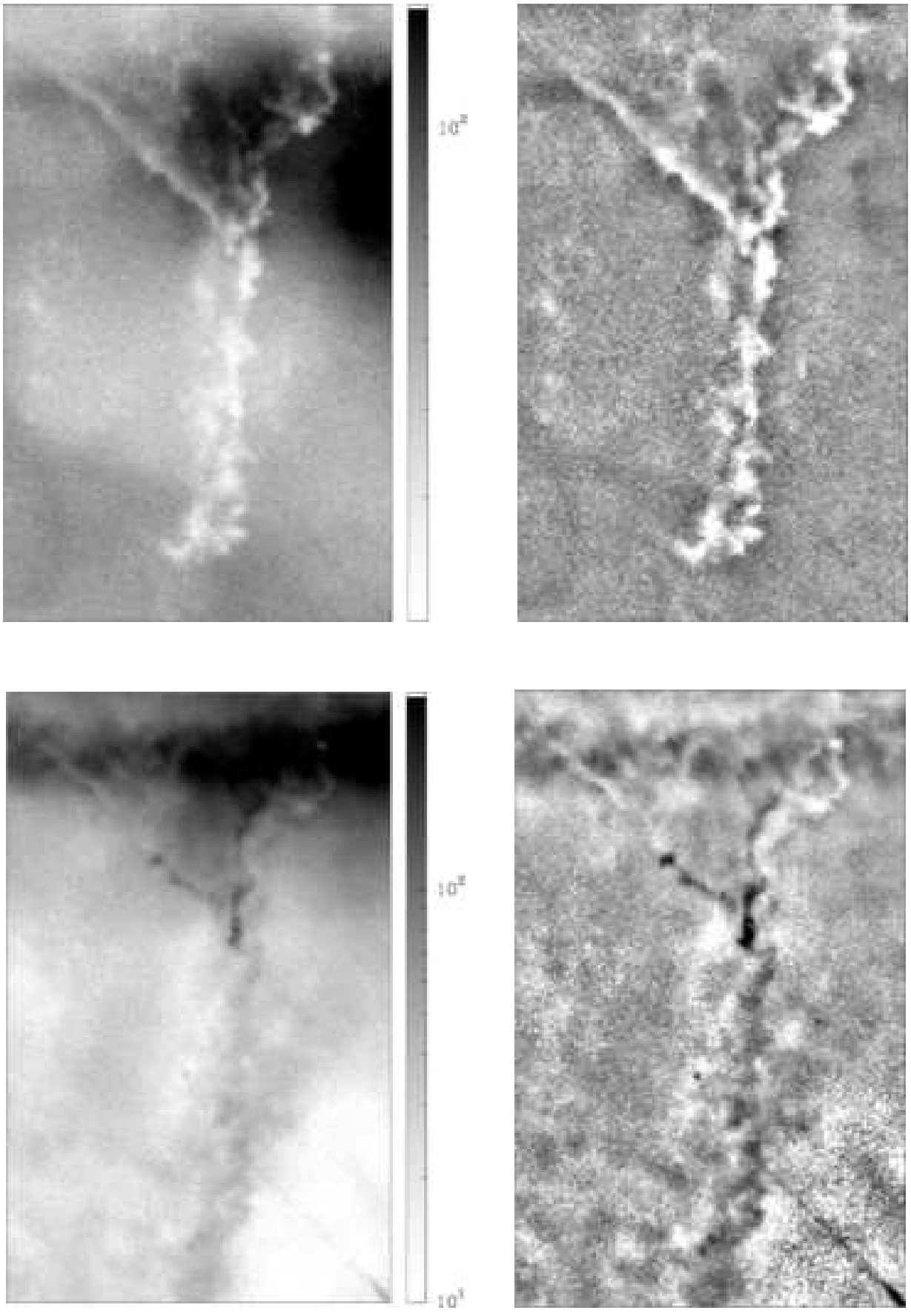
10^2
10^2
10^1

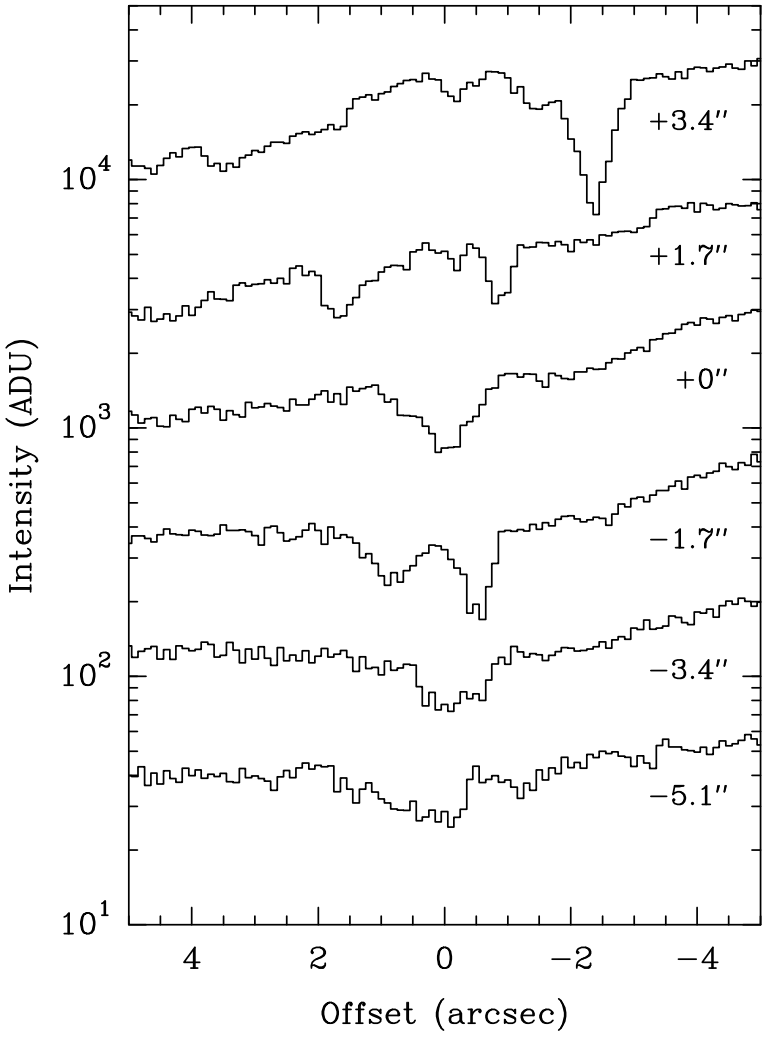
+3.4″
+1.7″
+0″
−1.7″
−3.4″
−5.1″
10^4
10^3
10^2
10^1
Intensity (ADU)
4
2
0
−2
−4
Offset (arcsec)

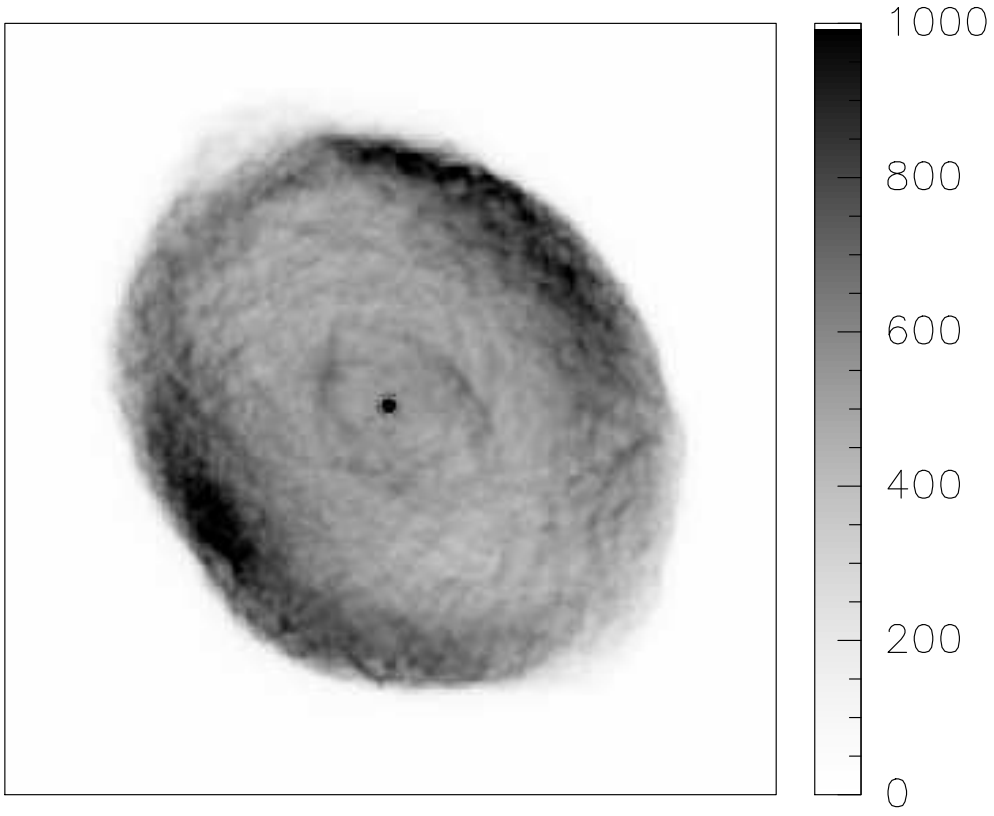
1000
800
600
400
200
0

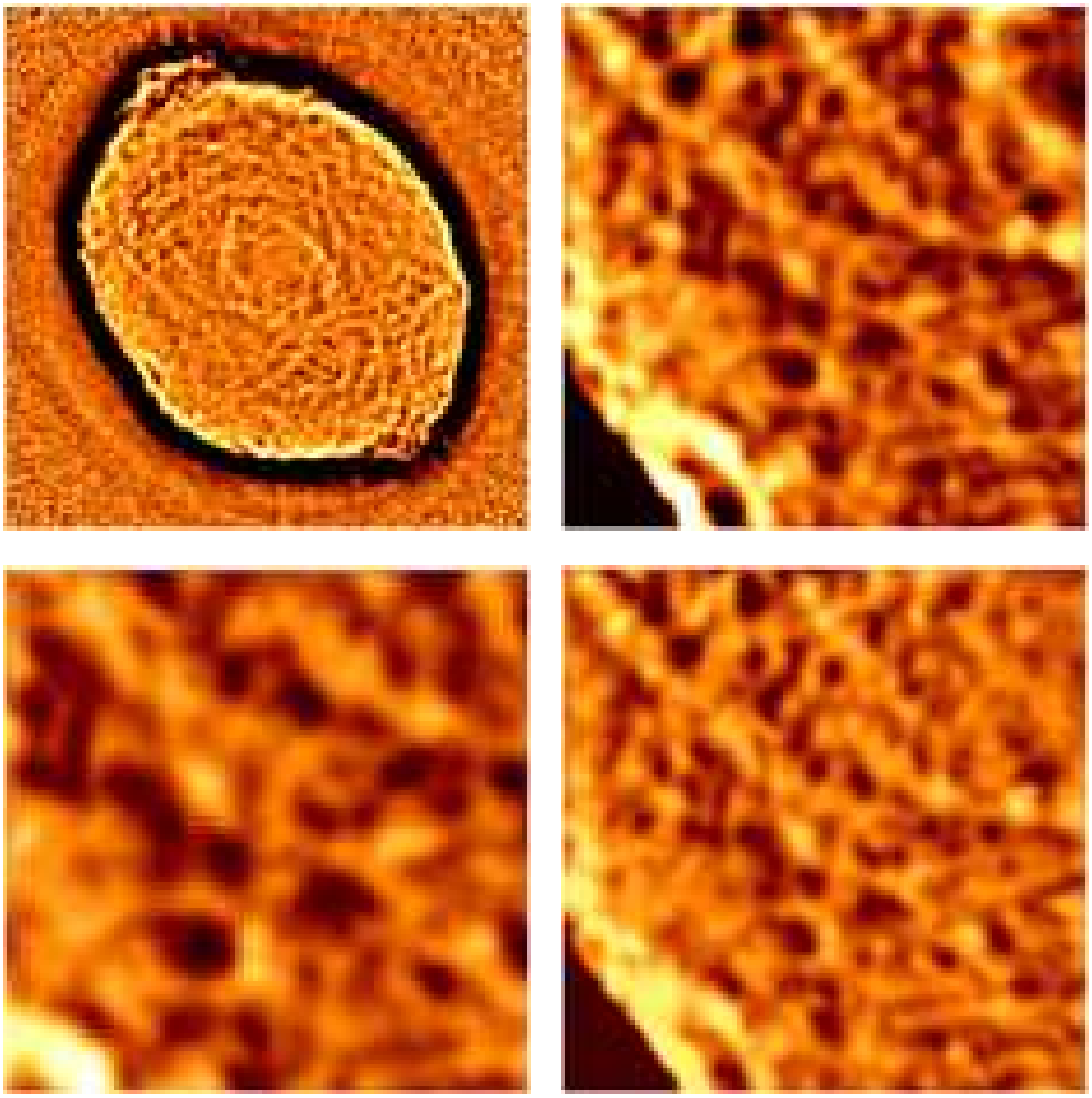

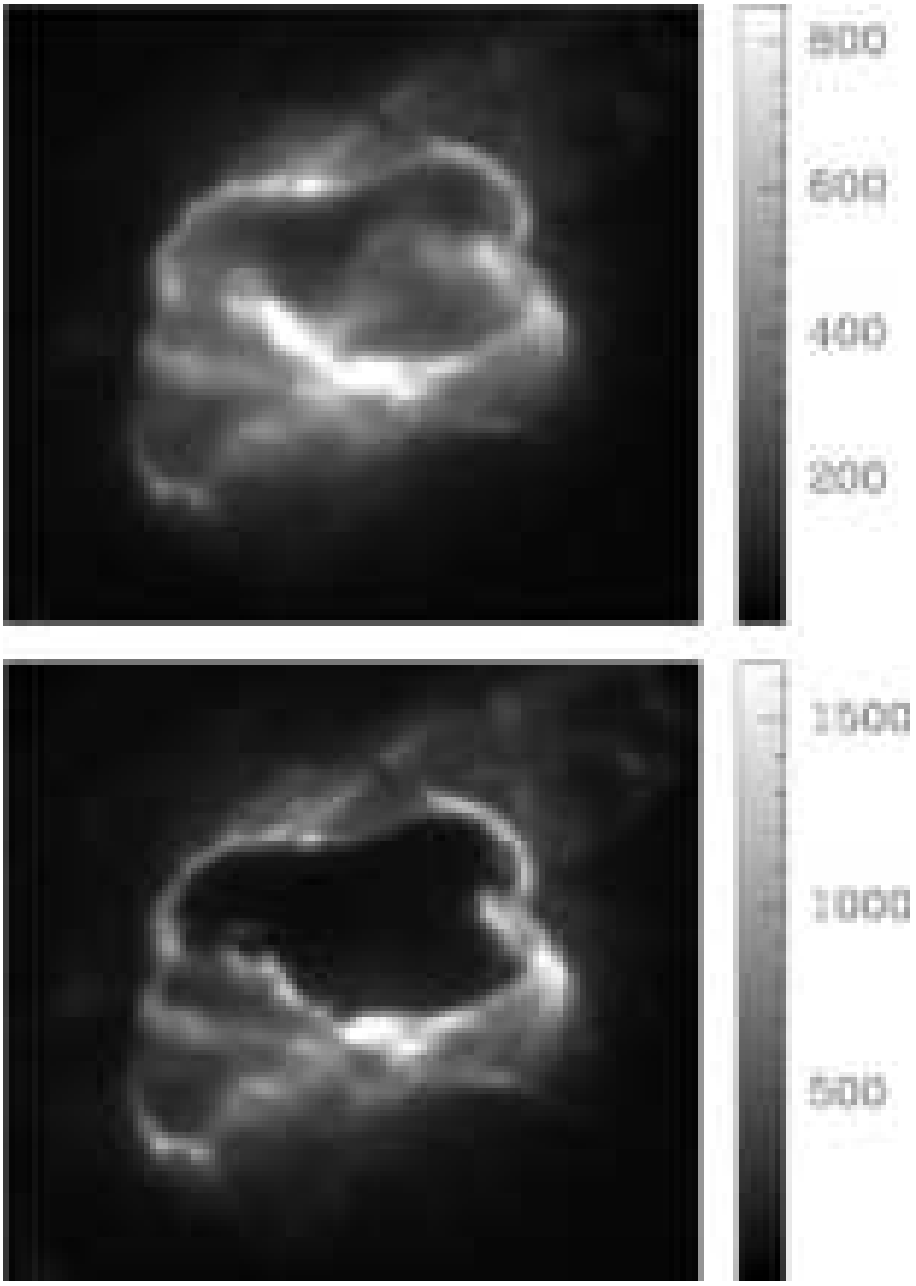
800
600
400
200
1500
1000
500

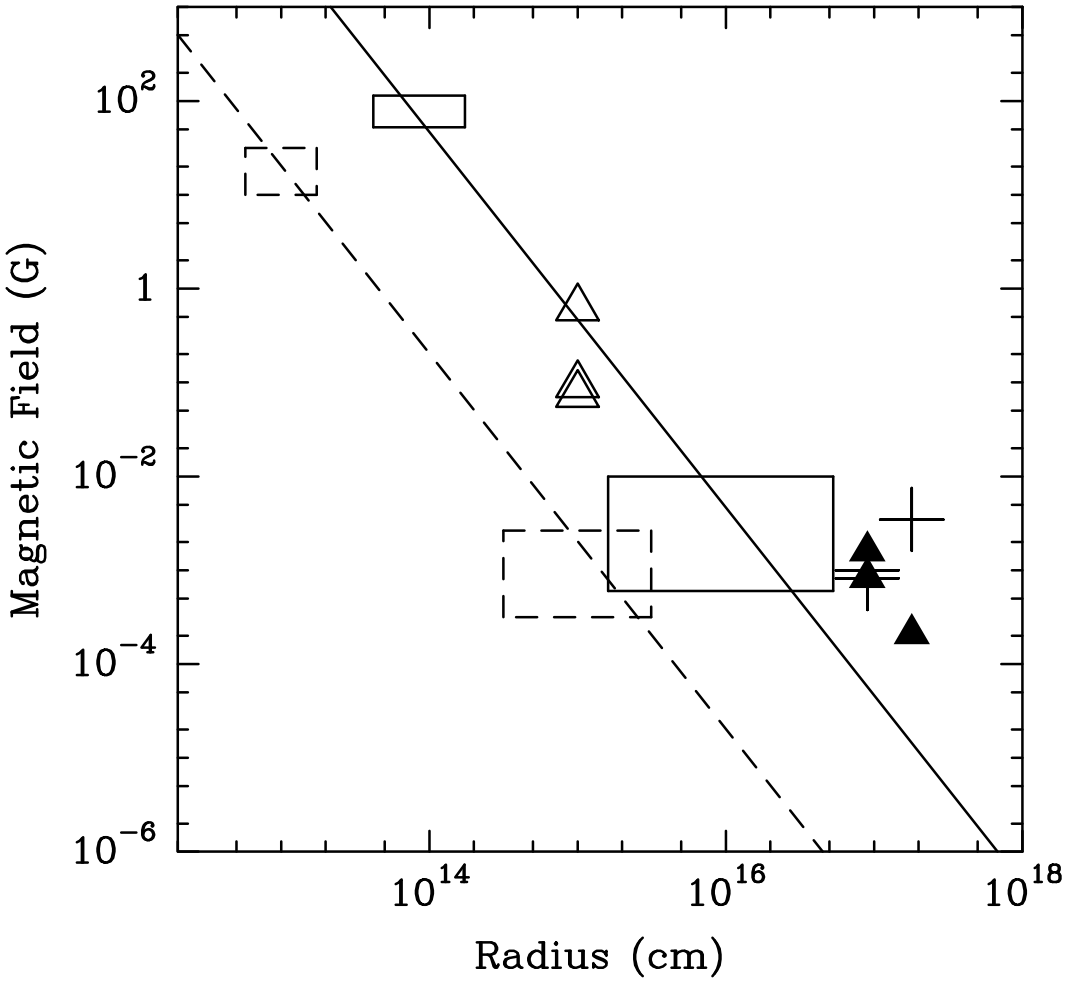
Magnetic Field (G)
10^2
1
10^{-2}
10^{-4}
10^{-6}
10^{14}
10^{16}
10^{18}
Radius (cm)